Ground Support 2023 – J Wesseloo (ed.)

doi:10.36487/ACG_repo/2325_29

Accelerated galvanic corrosion between graphitic rock from underground mines and metal coupons

C Stazick *Centers for Disease Control and Prevention, National Institute for Occupational Health & Safety, Spokane Mining Research Division, USA*

G Feagan *Centers for Disease Control and Prevention, National Institute for Occupational Health & Safety, Spokane Mining Research Division, USA*

S Sunderman *Centers for Disease Control and Prevention, National Institute for Occupational Health & Safety, Spokane Mining Research Division, USA*

Abstract

Dissimilar materials, such as steel and graphite, can experience galvanic corrosion resulting in safety hazards for many industries. Rock samples from a United States mine that exhibits electrochemical properties similar to graphite were galvanically coupled to corrosion coupons in an accelerated environment. Traditional weight loss and potentiostatic measurements were utilised to investigate the rock's observed in situ influence on metal comparable to underground support (e.g. rockbolts or steel mesh). Corrosion rates of the galvanically coupled coupons were multiple times higher than the coupons in the standard solution alone, with coupons held at higher temperature and humidity experiencing the most aggressive degradation over the testing period. Surface analysis of samples revealed extensive pitting of the steel, resembling failed bolt samples from partner mines. Metallic ground support in contact with graphitic rock has a higher potential for severe corrosion rates that could lead to premature failure of the ground support and ultimately pose a safety threat to mine workers without intervention.

Keywords: *corrosion, galvanic corrosion, metal ground support*

1 Introduction

Corrosion of metal is a dangerous and costly reaction that impacts almost all industries. In mining, metal ground support is subjected to a wide range of conditions that enable multiple types of corrosion. Steel rockbolts are widely used in in excavations to provide reinforcement, specifically for their low cost and high shear and tensile strength. At the time of installation, bolts support up to their load bearing capacity, which can be greatly reduced overtime from the effects of corrosion.

Corrosivity classification methods are continuing to be developed for mining operations, yet it is difficult to quantify contributing factors. These site evaluations typically consider atmospheric and groundwater measurements along with rock mass observations to classify the corrosivity of a section established by Hassell (2008). Rock mass properties should be considered for corrosion contribution in support design stages to avoid extensive rehabilitation and potential safety concerns. This study focuses on the presence of presumed graphitic minerals contained in host rock from a northern United States metal mine. Although well-crystallised graphite, which is a form of stable elemental carbon, is uncommon, materials containing dispersed graphitic carbon are present in many deposits. Galvanic coupling of this graphitic host rock with steel and its resulting effects on the corrosion rate are investigated in this analysis.

Galvanic corrosion occurs when two dissimilar conducting materials are in contact and in a common electrolyte, allowing current and electrons to flow between them. The galvanic series indicates the direction of flow and the likelihood of a galvanic coupling. Graphite is one of the most noble (cathodic) conductors, while steel is less noble (anodic) in the same reference electrolyte. When galvanically coupled to each other, steel is oxidised, while the graphite is reduced and protected by the steel. This results in the degradation of

steel in contact with this material. Figure 1 shows an example of heightened corrosion of mesh support at contact points with the graphitic rock mass.

Figure 1 Observed galvanic corrosion in partner mine where metal ground support contacts the graphite-like rock

The time of wetness and salinity of electrolytes that pass through the rock mass has a great effect on the extent of corrosion for these materials, as described in an article by Roy et al. (2016). In situ observations have shown that the galvanic corrosion level is low in areas with dry host rock and increases in more saturated areas.

Corrosion between graphite composites or carbon fibre materials and metal has been observed in construction, aerospace, automotive, and rehabilitation industries. Although limited, initial research by Miller (1975) investigated corrosion rates of various metals coupled to graphite epoxy materials using electrochemical techniques and provided information for pure graphite. Recent research by Song et al. (2021) has extended to the galvanic corrosion between certain metals and carbon-fibre-reinforced polymers. Lui et al. (2022) also published on the interaction between graphite grounding electrodes and zinc-plated steel grounding straps. Few studies have currently been conducted for soil or rock environments, leaving a gap for the mining industry.

2 Methodology

2.1 Experimental set-up

This study researches the effect of galvanic corrosion on mild steel coupons in both ambient and accelerated corrosion conditions (high heat and humidity). The influence of high carbon conductive mine rock on the galvanic corrosion rate of mild steels was quantified for both environments through traditional mass loss measurements and compared to the corrosion rate of coupons that were not galvanically coupled to rock through electrochemical testing methods.

Rock samples from a United States partner mine were processed into rectangular sections of equal area for both testing conditions. The rock sample was sized to have a 1:1 surface area ratio with the total number of metal coupons. Two identical apparatuses were made to hold five coupons and one rock sample in a common electrolyte, as well as to have them electrically connected for galvanic coupling. This set-up can be seen in Figure 2. Pieces of ultra-low resistivity carbon foam were placed in contact with rock and a copper plate above that to provide a good electrical connection between the rock and coupons. The coupons were

attached to a moveable copper arm that allowed them to be removed as needed. Coupons for the ambient condition were labelled 1–5, while the accelerated test coupons were labelled 6–10.

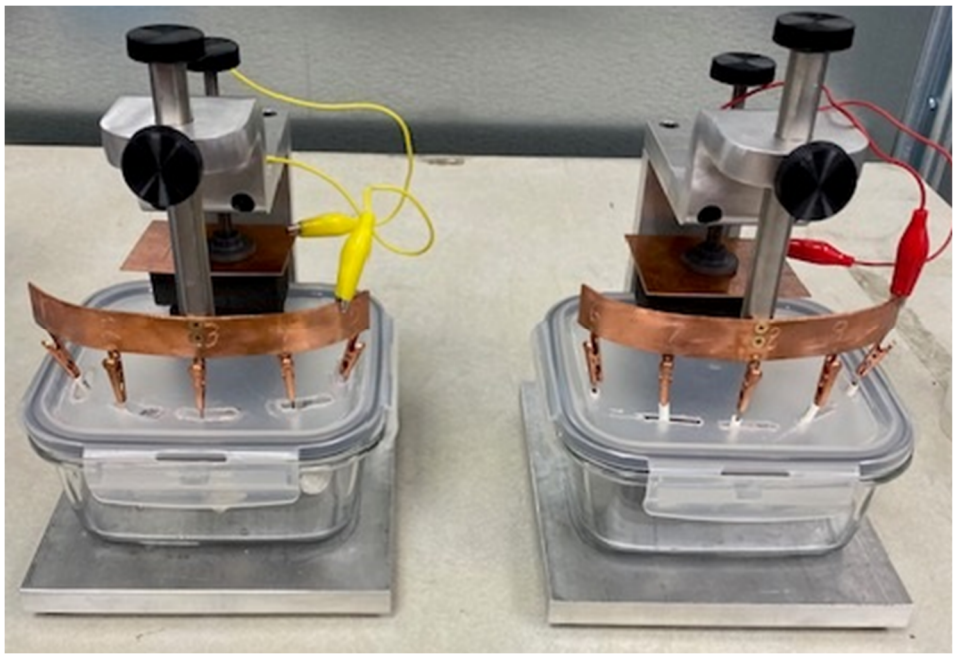

Figure 2 Testing apparatuses used for long-term coupon testing. The left set-up held coupons 1–5 in ambient conditions, and the right set-up held coupons 6–10 in the environmental chamber

Mild carbon steel coupons were machined, weighed, and had a tail of the same composition spot welded onto them. The weld joint was epoxied to help reduce crevice or other types of corrosion at that location. Once the coupons were placed in the assemblies in Figure 2, a wire was used to electrically connect the rock sample to them. The glass container that the rocks and coupons were submerged in was then filled with a standard 0.1 M NaCl solution. This concentration was chosen to approximate the average chloride concentration present in the affected underground mine areas from which the rock samples were collected. Water samples from both mines were obtained by rubbing de-ionised water into boreholes in the rock body and diluting them to 100 mL.

One assembly was placed on a countertop for the duration of the test at ambient conditions, while the other was placed in an environmental chamber to accelerate the corrosion. The chamber was held at approximately 48.8°C and 90% humidity, which are both factors known to increase the rate of corrosion. This temperature was chosen to accelerate the corrosion of the coupons and to match rock mass temperatures that have been observed in some partner mines. Prior studies described by Heidersbach (1990) show that the corrosion rate of low carbon steel in sea water doubles for a 30°C increase in temperature, until the trend plateaus at approximately 80°C. This correlation could be used to scale rates for observed in situ corrosion. Above this temperature, the system reaches the boiling point of the water and the dissolved oxygen level drops.

2.2 Electrochemical testing

Electrochemical measurements were taken using a potentiostat to obtain baseline corrosion rates for the steel coupons in the standard salt solution. The coupons were inserted into a ‘paint cell,’ as seen in Figure 3. These cells are commonly used to test bare metal samples.

Figure 3 Paint cell used for electrochemical tests to obtain the baseline corrosion rate of a coupon in the standard solution

To obtain these baseline corrosion rates, linear polarisation resistance (LPR) scans were performed. LPR scans provide a non-destructive testing method to obtain corrosion rate data. This is achieved by polarising the material +/-10 mV around its open circuit potential, resulting in the material's resistance to polarisation being measured, as detailed by Gamry Instruments Inc. (n.d.). By applying the Stern–Geary equation, an estimated corrosion rate is provided. This was performed twice, once for each rock sample from the two assemblies. Figure 4 shows the LPR scan for the ambient assembly rock sample and fresh coupon.

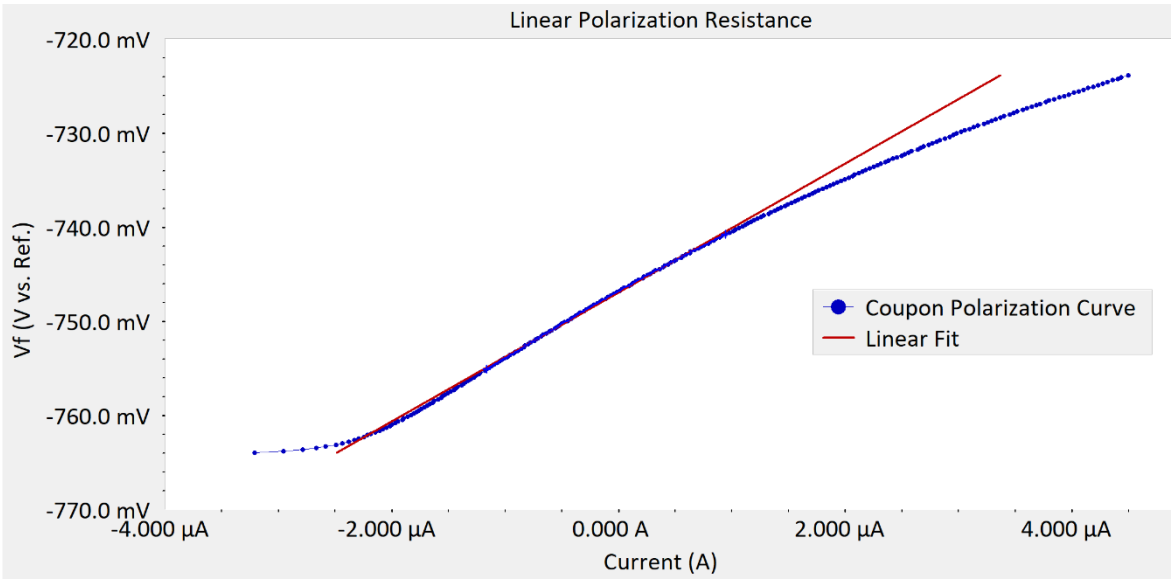

Figure 4 Linear polarisation resistance test scan for the control coupon corrosion rate

Zero-resistance ammeter (ZRA) scans were also performed using a 'para-cell' to gather a reference galvanic corrosion rate between a coupon and the individual rock samples used for both the ambient and environmental chamber environments. In ZRA, a voltage is applied to one material, the working electrode, to maintain both materials in the system at the same potential. The applied current of the source is measured and reported (Jones 1996). The corresponding corrosion rate was calculated using Equation 1:

$$CR = 0.00327 \times \frac{(i_{corr} \times EW)}{(A \times D)} \quad (1)$$

where:

CR = corrosion rate in millimetres per year (mm/y).

i_{corr} = corrosion current (μA).

EW = equivalent weight of material.

A = area (cm^2).

D = density (g/cm^3).

2.3 Coupon analysis

A coupon from each assembly was removed at varying time intervals to be cleaned, weighed, and imaged for analysis. Replacement coupons were inserted in their place to maintain the rock-to-coupon area ratio. After removal, coupons were left to dry for 48 hours and corrosion products were gently removed. ASTM Standard G1–03 (ASTM International 2017) was followed using 12 M hydrochloric acid (HCl) followed by ultrasonic cleaning in multiple cycles until the coupon weight stabilised.

Once the final weight was obtained, the corrosion rate was calculated using Equation 2:

$$CR = \frac{(K \times W)}{(A \times T \times D)} \quad (2)$$

where:

CR = corrosion rate (mm/y).

K = a constant = 8.76×10^4 for mm/y.

W = mass loss (grams).

A = area (cm^2).

T = time of exposure (h).

D = density (g/cm^3).

After cleaning, coupons were imaged using a scanning electron microscope (SEM) at two different magnifications to qualitatively analyse the surface structure and the degradation of coupons over time. Images were captured at both the 200 and 500 μm scale.

3 Data

Data for the baseline and long-term coupon corrosion rates and SEM images are detailed below.

3.1 Baseline coupon corrosion rate

The corrosion rates for both the ambient and environmental chamber control coupons were calculated using Gamry Echem Analyst™ (Gamry Instruments Inc. 2022). From the LPR scan, the baseline corrosion rate of a metal coupon in the standard salt solution was 0.0638 mm/y, when not galvanically coupled to the rock samples.

Using the ZRA scans, both rock samples were tested for their galvanic corrosion rate. The ambient assembly rock had a galvanic corrosion rate with the coupon of 0.822 mm/y and the environmental chamber assembly rock sample was 0.842 mm/y. Both ZRA scans were run at ambient conditions to gain an instantaneous corrosion rate and do not reflect the temperature and humidity conditions for the environmental chamber coupons.

3.2 Long-term coupon corrosion rates

For the long-term coupons, the time in testing, weight changes, and corrosion rates are reported in Table 1.

Table 1 Weight lost data for long-term coupons. Coupons 1–5 were at ambient conditions and 6–10 in the environmental chamber

Coupon	Time (h)	Initial weight (g)	Final weight (g)	Mass loss (g)	Mass loss (%)	Corrosion rate (mm/y)
1	1,054	4.29794	4.09834	0.19959	4.644	0.705
2	3,186	4.29540	3.79089	0.50451	11.75	0.589
3	4,460	4.30629	3.60726	0.69903	16.23	0.583
4	5,231	4.38758	3.51527	0.87231	19.88	0.621
5	5,901	4.30149	3.70946	0.59203	13.76	0.373
6	1,054	4.31443	3.89856	0.41587	9.639	1.468
7	3,186	4.37872	2.99599	1.38273	31.58	1.615
8	4,460	4.29812	2.04039	2.25773	52.53	1.884
9	5,231	4.38026	1.28980	3.09046	70.55	2.198
10	5,901	4.48729	2.49238	1.99491	44.46	1.258

The percent mass loss for each coupon was graphed against time in testing, as shown in Figure 5.

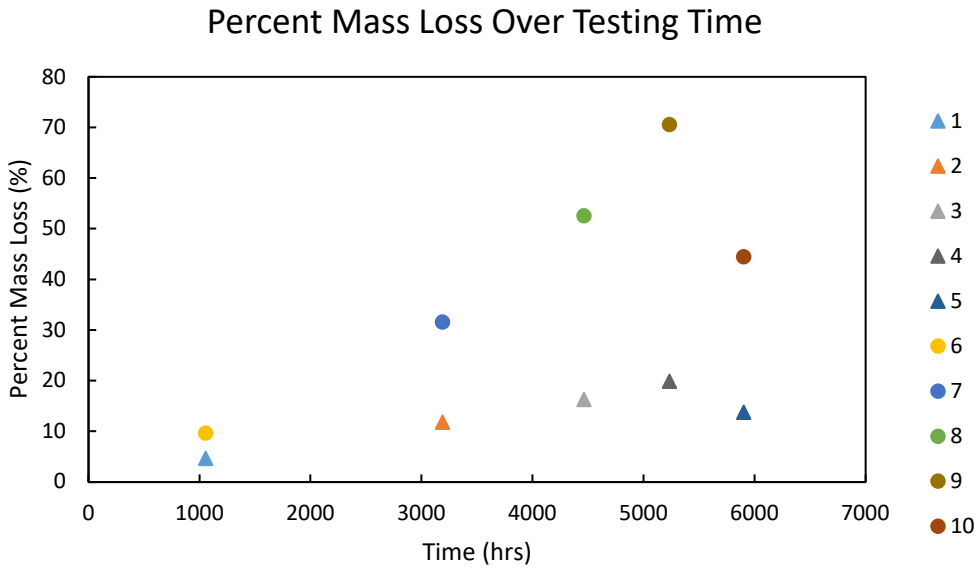

Figure 5 Scatter plot of the percent mass loss during the test duration. Coupons 1–5 were at ambient conditions and 6–10 in the environmental chamber

Table 2 shows the comparison of the corrosion rate of the coupons galvanically coupled to the mine rock to the control coupon corrosion rate from the LPR scan.

Table 2 Ratio of the corrosion rate of the long-term coupons versus the corrosion rate of the control coupon baseline

Coupon	Corrosion rate coupon: control corrosion rate (ratio)
1	33.7
2	28.2
3	27.9
4	29.6
5	17.8
6	70.1
7	77.2
8	90.0
9	105.0
10	60.1

3.3 Scanning electron microscope analysis

Figure 6 shows the initial surface structure of a coupon prior to long-term corrosion testing. Over the time of testing, the change of structural integrity of the coupons can be seen through the SEM images.

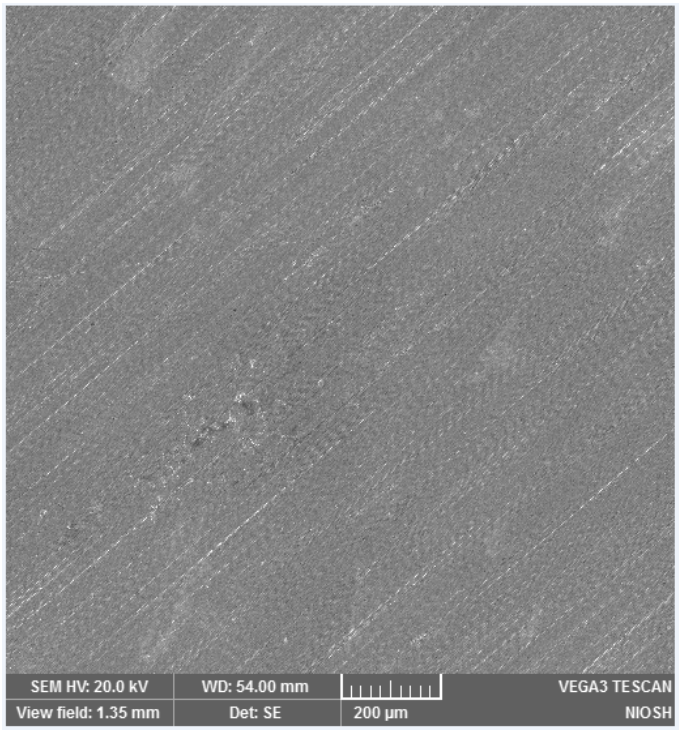

Figure 6 Scanning electron microscope control image of a coupon before the long-term corrosion testing began

Figure 7 shows a representative of the high corrosion rate of the environmental chamber coupons 6–9 over time.

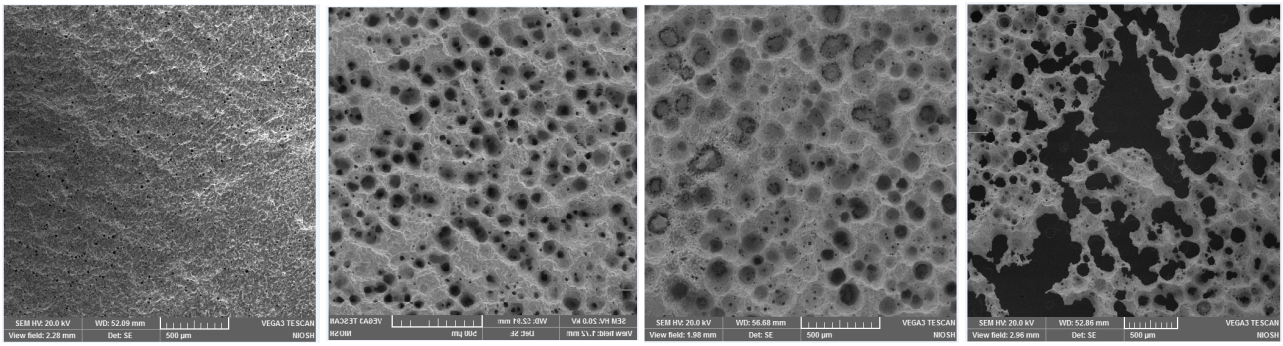

(a) (b) (c) (d)

Figure 7 (a) Coupon 6 – 1,054 hours in testing; (b) Coupon 7 – 3,186 hours in testing; (c) Coupon 8 – 4,460 hours in testing; (d) Coupon 9 – 5,231 hours in testing

Figure 8 shows a comparison of coupons 2 and 7 at the 200 µm scale, which were in testing the same amount of time.

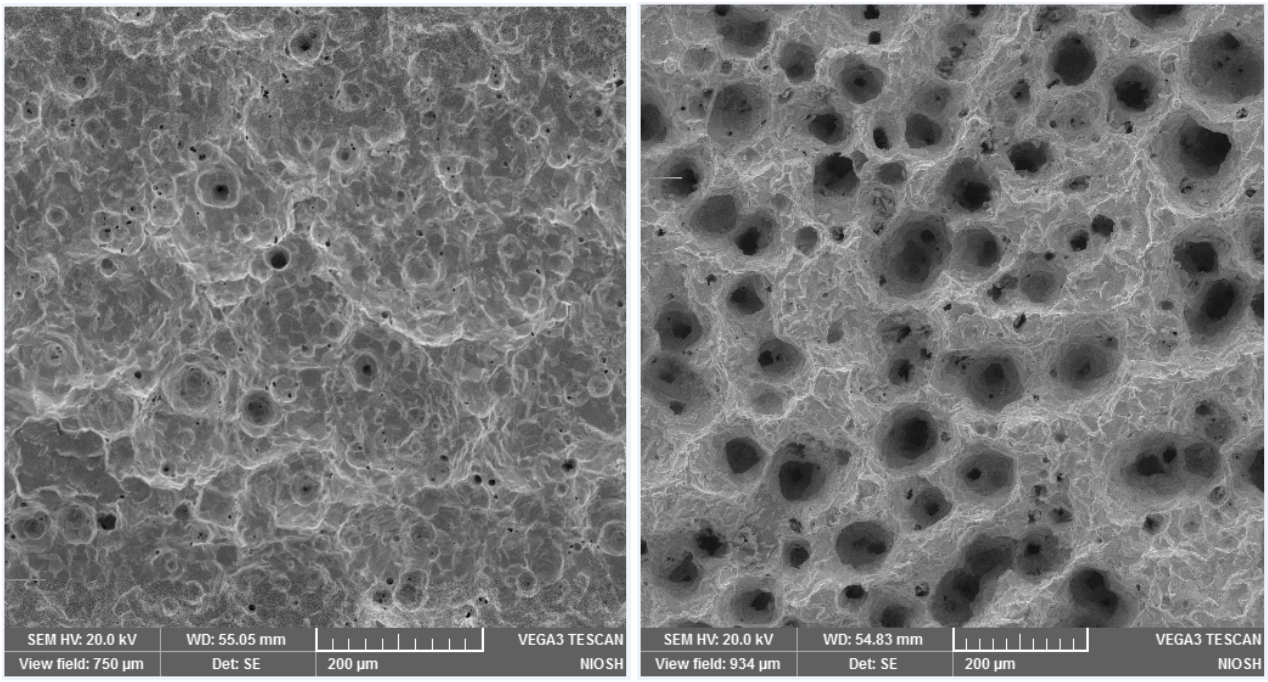

(a) (b)

Figure 8 (a) Coupon 2 from ambient test environment; (b) Coupon 7 from the environmental chamber environment

4 Results

Results for the baseline and long-term coupon corrosion rates and SEM images are detailed in the following sections.

4.1 Baseline coupon corrosion rates

Using the LPR potentiostat data, the baseline control coupon corrosion rate in the standard solution was very low at 0.0638 mm/y. When compared to the ZRA scans using the same device for a galvanic couple, the corrosion rate was approximately 39 times higher than when the coupon was not in a coupling with the mine rock. This aligns with in situ observations of ground support in partner mines, which visibly have much greater

corrosion at contact sites of mesh and bolts with the rock. Figure 9 shows an example of heightened corrosion at sites where the mesh is physically contacting the rock mass.

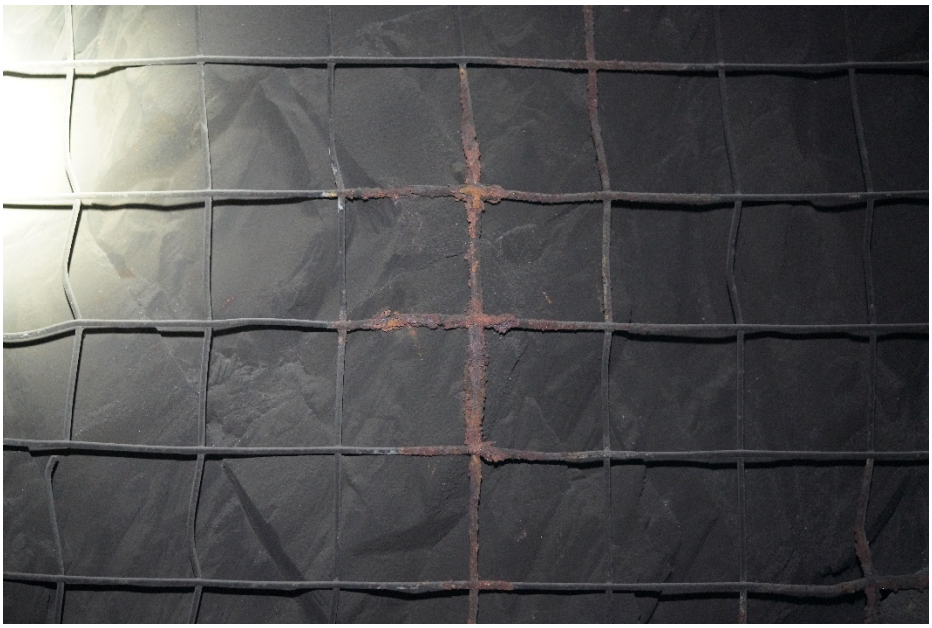

Figure 9 Coated mesh with increased corrosion at contact points with graphite-like rock

4.2 Long-term coupon corrosion rates

For the same time in testing, the coupons that were in the accelerated environment had a higher percent mass loss and corrosion rate than the coupons held at ambient conditions. This was expected as temperature heavily affects corrosion rates along with humidity in relation to time of wetness. The corrosion rate of the environmental chamber coupons was roughly 2.08 to 3.54 times higher than the ambient coupons, which is reflective of a roughly 20°C temperature difference. In many mine environments, metal ground support will be placed in rock masses with this temperature or greater.

The corrosion rates in Table 1 are reported in mm/y, with the highest rate being 2.2 mm/y. A standard hollow friction bolt is approximately 2.46 mm thick in the United States, indicating that it would corrode through in two years if the rate remained constant in this environment. Inflatable bolts are generally 2 mm thick and would corrode at a similar rate. Figure 10 below shows an inflatable bolt that failed pull testing less than two years after installation in a partner mine. It should be noted that the highest experimental corrosion rates were held at conditions to encourage accelerated corrosion, so in situ rates may be lower depending on the temperature and humidity of the environment.

Figure 10 Failed bolt from a partner mine where metal ground support contacts the graphite-like rock

Figure 5 graphically shows the difference in percent mass loss for the coupons in the two testing environments. As expected, the ambient coupons consistently had lower mass loss than the environmental chamber coupons. Although coupons 4 and 9 were in testing for less time than coupons 5 and 10, the percent mass loss, and subsequently the corrosion rates, were higher for coupons 4 and 9. This could be attributed to the four newer replacement coupons in each testing apparatus drawing more corrosion current over coupons 5 and 10, which would have large amounts of corrosion products at that point in testing. The corrosion rate of metal typically decreases over time as the metal degrades versus a fresh piece of steel. This results from the corrosion products creating a protective layer that reduces the ability of oxygen to diffuse to the surface of the metal, amongst other factors that cause the rate to slow over time as described in an article by Fan et al. (2020).

Corrosion rates for the ambient test coupons over the entire test averaged to 0.574 mm/y, which is in a reasonable range when compared to the ZRA corrosion rate of 0.842 mm/y. Both tests were operated at similar temperature and humidity conditions; however, the ZRA test was performed on a fresh metal coupon, compared to those in testing whose rate would mostly likely decrease over time. ZRA testing also provides instantaneous corrosion rates and cannot be continually run over a long time interval, unlike the long-term coupon tests.

When the corrosion rate of the coupons galvanically coupled to the mine rock were compared to the control coupon rate, the difference was extremely large. For the ambient coupons, the corrosion rate when coupled was 17.8 to 33.7 times higher than when not coupled. For the environmental chamber coupons, the corrosion rate when coupled was 60.1 to 105 times higher than when not coupled, as seen in Table 2. This variance in corrosion rates is significant and may lead to expedited degradation of metal ground support in some mine environments.

4.3 Scanning electron microscope analysis

For all coupons in testing, SEM analysis revealed extensive surface degradation as coupons remained in the galvanic couple over time. Using measurement tools, corrosion pits on the surface averaged 14 µm for the first coupons removed from the testing environments and increased up to 200 µm for the later coupons. Coupon 9 from the environmental chamber experienced extreme metal loss, with the centre becoming almost bare. When qualitatively comparing the coupon images, Figure 7 shows the progression of corrosion at the 500 µm scale. The quantity and size of corrosion pits visibly increases as the time in testing increased. Between the two different long-term testing environments, Figure 8 shows the contrast in level of corrosion between the ambient and environmental chamber conditions. Coupon 2 had a corrosion rate of 0.589 mm/y,

while coupon 7's rate was 1.61 mm/y. There was almost a 20% difference in their mass loss over the 3,186-hour period, as seen in Figure 5.

5 Conclusion

Graphitic behaving mine rock qualitatively and quantitatively can form a galvanic couple with various types of steel representative of underground mine support. Corrosion rates of mild steel coupons were 39 times higher than the steel alone using potentiostatic testing, and up to 105 times higher through mass loss calculations of the long-term tests. In higher temperature and humidity environments, the galvanic corrosion rates were approximately 2–3.5 times higher than at ambient conditions, which was also qualitatively seen through SEM imaging for coupons in testing for the same amount of time. Without considering the electrochemical properties of the host rock, ground support may be susceptible to accelerated galvanic corrosion, leading to potential safety hazards for mine employees.

It must be noted that this conclusion is based on laboratory studies that reflect observed in situ corrosion, but it should be confirmed through field testing. The findings in this paper represent galvanic corrosion rates for underground mine support metals, but do not comprehensively consider all methods of corrosion that could have any effects on the support. Future work for galvanic corrosion in the mining environment could involve ways to physically and electrically isolate support from the rock mass, potential cathodic protection, or other materials better suited for the mining environment.

Disclaimer

The findings and conclusions in this report are those of the author/s and do not necessarily represent the official position of the National Institute for Occupational Safety and Health (NIOSH), Centers for Disease Control and Prevention (CDC). Mention of any company or product does not constitute endorsement by NIOSH, CDC.

References

ASTM International 2017, *Standard Practice for Preparing, Cleaning, and Evaluating Corrosion Test Specimens (ASTM G1-03)*, ASTM International, West Conshohocken.

Fan, Y, Lui, W, Li, S, Chowwanonthapunya, T, Wongpat, B, Dong, B, ... Li, X 2020, 'Evolution of rust layers on carbon steel and weathering steel in high humidity and heat marine atmospheric corrosion', *Journal of Materials Science & Technology*, vol.39, pp. 190–199, https://doi.org/10.1016/j.jmst.2019.07.054

Gamry Instruments Inc. 2022, *Gamry Echem Analyst,* computer software, Gamry Instruments Inc., Warminster.

Gamry Instruments Inc. n.d., *Polarization Resistance Tutorial – Getting Started,* viewed 3 March 2023, Gamry Instruments Inc., Warminster, https://www.gamry.com/application-notes/corrosion-coatings/corrosion-techniques-polarization-resistance/

Hassell, R 2008, *Corrosion of Rock Reinforcement in Underground Excavations*, PhD Thesis, Western Australian School of Mines, Kalgoorlie.

Heidersbach, RH 1990, 'Marine corrosion', in *Metals Handbook*, 9th edn, ASM International, Ohio, pp. 893–926.

Jones, DA 1996, 'Galvanic and concentration cell corrosion', in B Stenquist & R Kernan (eds), *Principles and Prevention of Corrosion*, 2nd edn, Prentice-Hall Inc, Upper Saddle River, pp. 179–183.

Lui, L, Li, J, Peng, M, Li, W & Lei, B 2022, 'Macro-galvanic corrosion of tower grounding device consisting of graphite and Zn-coated steel in a simulated soil environment', *Engineering Failure Analysis*, vol. 135, https://doi.org/10.1016/j.engfailanal.2022.106136

Miller, BA 1975, *The Galvanic Corrosion of Graphite Epoxy Composite Materials Coupled With Alloys*, PhD Thesis, Air Force Institute of Technology Wright-Patterson Air Force Base, Dayton.

Roy, JM, Preston, R & Bewick, RP 2016, 'Classification of aqueous corrosion in underground mines', *Rock Mechanics and Rock Engineering*, vol.49, no.8, https://doi.org/10.1007/s00603-016-0926-z

Song, G-L, Zhang, C, Chen, X & Zheng, D 2021, 'Galvanic activity of carbon fiber reinforced polymers and electrochemical behavior of carbon fiber', *Corrosion Communications*, vol.1, pp. 26–39, https://doi.org/10.1016/j.corcom.2021.05.003